

# Measurement of Zone Plate Efficiencies in the Extreme Ultraviolet and Applications to Radiation Monitors for Absolute Spectral Emission

John Seely<sup>\*a</sup>, Glenn Holland<sup>b</sup>, James C. Bremer<sup>c</sup>, Tim Zukowski<sup>c</sup>, Michael Feser<sup>d</sup>, Yan Feng<sup>d</sup>,  
Benjawan Kjornrattanawanich<sup>e</sup>, and Leonid Goray<sup>f</sup>

<sup>a</sup>Space Science Division, Naval Research Laboratory, Washington DC 20375;

<sup>b</sup>SFA Inc., 2200 Defense Highway, Suite 405, Crofton MD 21114;

<sup>c</sup>Swales Aerospace, 5050 Powder Mill Road, Beltsville MD 20705;

<sup>d</sup>Xradia Inc., 4075-A Sprig Drive, Concord, CA 94596;

<sup>e</sup>USRA and NSLS, Brookhaven National Laboratory, Upton NY 11973;

<sup>f</sup>International Intellectual Group Inc., P. O. Box 335, Penfield NY 14526

\*john.seely@nrl.navy.mil

## ABSTRACT

The diffraction efficiencies of a Fresnel zone plate (ZP), fabricated by Xradia Inc. using the electron-beam writing technique, were measured using polarized, monochromatic synchrotron radiation in the extreme ultraviolet wavelength range 3.4-22 nm. The ZP had 2 mm diameter, 3330 zones, 150 nm outer zone width, and a 1 mm central occulter. The ZP was supported by a 100 nm thick Si<sub>3</sub>N<sub>4</sub> membrane. The diffraction patterns were recorded by CMOS imagers with phosphor coatings and with 5.2 μm or 48 μm pixels. The focused +n orders (n=1-4), the diverging -1 order, and the undiffracted 0 order were observed as functions of wavelength and off-axis tilt angle. Sub-pixel focusing of the +n orders was achieved. The measured efficiency in the +1 order was in the 5% to 30% range with the phase-shift enhanced efficiency occurring at 8.3 nm where the gold bars are partially transmitting. The +2 and higher order efficiencies were much lower than the +1 order efficiency. The efficiencies were constant when the zone plate was tilted by angles up to ±1° from the incident radiation beam. This work indicates the feasibility and benefits of using zone plates to measure the absolute EUV spectral emissions from solar and laboratory sources: relatively high EUV efficiency in the focused +1 order, good out-of-band rejection resulting from the low higher-order efficiencies and the ZP focusing properties, insensitivity to (unfocused) visible light scattered by the ZP, flat response with off-axis angle, and insensitivity to the polarization of the radiation based on the ZP circular symmetry. EUV sensors with Fresnel zone plates potentially have many advantages over existing sensors intended to accurately measure absolute EUV emission levels, such as those implemented on the GOES N-P satellites that use transmission gratings which have off-axis sensitivity variations and poor out-of-band EUV and visible light rejection, and other solar and laboratory sensors using reflection gratings which are subject to response variations caused by surface contamination and oxidation.

**Keywords:** Fresnel zone plate, extreme ultraviolet, diffraction, solar monitor

## 1. INTRODUCTION

A fundamental requirement for understanding and predicting solar variability and the effects of solar radiation on space weather and Earth climate is the accurate measurement of the radiation emissions from the Sun. While the Sun is brightest in the visible, the fainter and highly variable extreme ultraviolet (EUV) radiation can play a dominant role in heating the ionosphere, disruption of communications and navigation signals, and drag on satellites in low orbits. The present N series of Geostationary Operational Environmental Satellites (GOES-N) have solar monitors intended to accurately measure the absolute values of the total solar emissions in five EUV wavelength bands covering the 10 nm to 122 nm range. As shown schematically in Fig. 1, these instruments utilize transmission gratings for wavelength dispersion and silicon photodiode detectors with thin metal coatings to block the intense solar visible radiation scattered from the transmission grating and to attenuate out-of-band shorter wavelength radiation in the higher diffraction orders. Transmission gratings are composed of linear gold bars and open spaces and are not susceptible to contamination. In contrast, the more traditional reflection gratings are highly sensitive to surface contamination that can significantly alter the EUV reflectance and instrument throughput. Since it is desired to measure the Sun's EUV emission to 10% absolute

accuracy over a nominal 10-year operational lifetime after 5 years of on-orbit storage in space, reflection gratings were rejected in favor of transmission gratings for the GOES-N solar monitors.

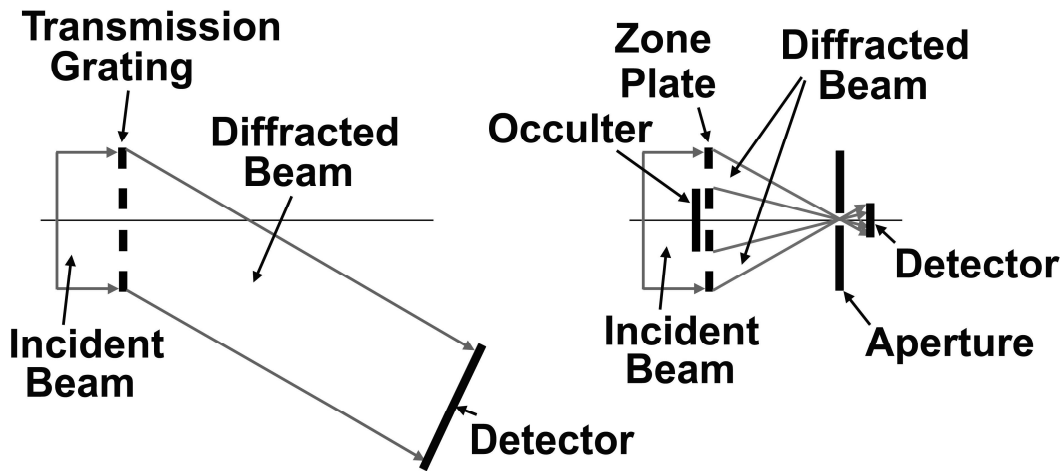


Fig. 1. Left: Schematic of the GOES-N solar monitor using a transmission grating. Right: Schematic of a solar monitor using a zone plate that focuses the radiation through a small aperture and onto a small-area detector.

The GOES-N solar monitors utilizing transmission gratings have a number of performance limitations that became apparent during the instrument calibration and testing phase:<sup>1</sup> (1) The thin filters on the two detectors for the 40-65 nm and 65-100 nm wavebands, Sn and In, have inadequate blocking of visible light scattered by the transmission grating (TG). (2) The TG has different efficiency for the two polarizations of the incident radiation (lower when the electric vector is perpendicular to the grating's gold bars and higher when parallel to the bars). (3) The TG efficiency changes with angle in the dispersion direction, and this results in variable instrument sensitivity across the  $0.5^\circ$  solar disk. (4) The TG has significant efficiency in the higher diffraction orders, and the out-of-band higher order, shorter wavelength radiation can generate signal levels comparable to the in-band signals in the 40-65 nm and 65-100 nm waveband ranges. (5) Because the TG does not focus the dispersed EUV radiation (see Fig. 1), the detector must have large area (typically  $1 \text{ cm}^2$ ) in order to generate adequate signal, and this makes the detector more sensitive to scattered visible light and more susceptible to contamination. The instrument modifications to correct some of these performance limitations have severely limited the ability of the GOES-N solar monitors to fulfill the original requirements for the accurate measurement of the absolute solar emission levels in wavebands covering the 10 nm to 122 nm EUV wavelength range.

Because of the now well-established limitations of transmission gratings for solar monitors, it was recently suggested that Fresnel zone plates can replace the transmission gratings in the next series of GOES-R solar monitors.<sup>2</sup> The schematic design of a ZP solar monitor is shown in Fig. 1. Because the zone plate (ZP) focuses radiation with its focal length inversely proportional to the wavelength, the solar image can be focused onto a detector at the selected EUV wavelength, and it is possible to utilize a small aperture over a small-area detector to establish the EUV waveband. The ZP focusing property allows implementation of a number of technical improvements: (1) Since the visible light scattered by the ZP is unfocused, it is substantially blocked by the small detector aperture while the desired EUV focused radiation passes through the aperture to the underlying detector. Thus the visible light blocking requirement for the thin metal filter on the detector can be relaxed. (2) Owing to the circular symmetry of the ZP, the ZP is insensitive to the polarization of the incident radiation. (3) The ZP efficiency is constant with off-axis angle because of circular symmetry. (4) The ZP higher-order efficiencies have been measured to be lower than those of transmission gratings, thus mitigating out-of-band contamination of the desired in-band EUV signal. (5) The small-area (mm size) detector, compared to the much larger (cm size) detector necessary in TG instruments, has low background (dark) signal and can measure smaller EUV radiation levels. This permits the use of a small wide-bandgap photodiode, such as SiC,<sup>3,4</sup> having negligible sensitivity to visible radiation (solar blind) and that may have higher dark signal and lower EUV sensitivity compared to

a silicon photodiode. In addition, the small aperture over the detector provides protection from contamination. Finally, because of very low visible light sensitivity, the apertured small-area detector can be placed close to the ZP, and the overall size and weight of the solar monitor can be much smaller than the present generation of GOES-N instruments using transmission gratings and relatively large detectors placed farther from the transmission gratings.

In support of the design and optimization of solar monitors using zone plates,<sup>1</sup> we present here the first detailed experimental characterization of zone plate properties, important for EUV solar monitors, in the wavelength range 3.4 nm to 22 nm. The measurements include the on-axis efficiencies in the focused and diverging orders as well as the off-axis efficiencies on the +1 order, the operating order in a solar monitor.

## 2. DIFFRACTION PATTERN IMAGES

The measurements were performed at the Naval Research Laboratory beamline X24C at the National Synchrotron Light Source, Brookhaven National Laboratory. The ZP was mounted on an x-z stage, where z was parallel to the incident radiation beam and along the axis to the detector assembly, and x was in the horizontal plane perpendicular this axis. The detector assembly was mounted on an x-y-z stage, and the two stages could be accurately moved under computer control. The ZP and detector assemblies were mounted on an x-y-yaw platform, and the yaw motion provided the ability to measure the efficiencies at off-axis angles.

The detector assembly consisted of two 1 cm<sup>2</sup> AXUV100 silicon photodiodes from IRD Inc, with 0.15 mm and 0.60 mm apertures, and two CMOS imagers with 5.2 μm and 48 μm pixels. The diffraction pattern produced by the ZP was first captured by the CMOS imager, and based on metrology of the images, a selected photodiode could be moved to a precise location in the ZP diffraction pattern under computer control. The efficiency was measured by centering the diode aperture in the focus of a converging (positive) order at a selected incident wavelength, as indicated schematically in Fig. 2, and dividing the diode current by the current produced by the direct beam when the ZP was moved aside. The efficiencies of the diverging (negative) orders and the undeflected zero order were determined from the images that were calibrated based on the diode efficiency measurement in the +1 order.

The ZP parameters are listed in Fig. 3. The outermost gold zone was 2 mm in diameter and 150 nm wide. The gold zones were mounted on a 100 nm thick Si<sub>3</sub>N<sub>4</sub> membrane, and the membrane was mounted on a silicon frame with 2.5 mm x 2.5 mm opening. The central occulter was 1 mm in diameter and was mounted on a fixture, separate from the ZP, using four support spokes. The entire ZP assembly was mounted on a flexure with a 3 mm hole. The flexure was used to initially orient the ZP perpendicular to the incident radiation beam.

Shown in Fig. 4 is the image of the diffraction pattern produced when illuminating the ZP with 13.5 nm radiation that overfilled the flexure 3 mm hole and the ZP assembly. Visible are the shadows of the various ZP structures, the undiffracted radiation transmitted through the Si<sub>3</sub>N<sub>4</sub> membrane outside the zones, the +1 focused order, undeflected 0 order, and the diverging -1 order appearing outside the diameter of the 3 mm hole.

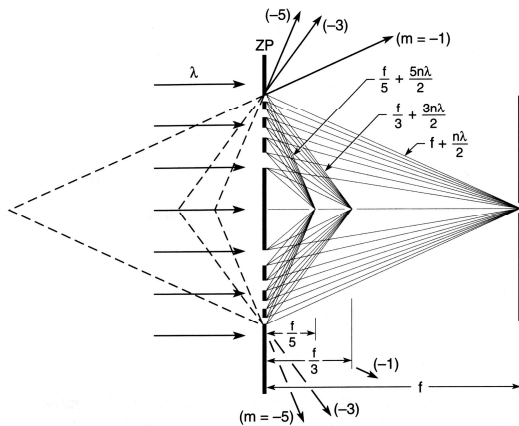


Fig. 2 Zone plate converging and diverging diffraction orders.

### Zone Plate Parameters:

Outer Diameter	μm	2000
Inner Diameter (no zones)	μm	1000
Outermost Zone Width	nm	150
Zone Material		Electroplated Gold
Zone Height	nm	180 +/- 10%
Number Of Zones <sup>2</sup>		3330
Suggested Energy Range <sup>3</sup>	keV	0.13-1.4
Theoretical Max. Diffraction Efficiency <sup>1</sup>	%	15 (@ 1.1 keV)
Support Membrane Material		Si <sub>3</sub> N <sub>4</sub>
Support Membrane Thickness	μm	0.1
Support Membrane Size	mm	2.5 x 2.5
Support Silicon Frame Size	mm	6 x 6
Central Stop Diameter <sup>4</sup>	μm	1000
Central Stop Height / Material	μm	500/stainless steel

<sup>1</sup> The guaranteed focusing efficiency for condenser zone plates is 50% of the theoretically calculated value.

<sup>2</sup> Number of fabricated rings calculated for a full zone plate (no missing inner zones).

<sup>3</sup> Energy range for which the theoretical efficiency is greater 10%.

<sup>4</sup> The stop for the condenser is a EDM-cut stainless steel plate.

Fig. 3. The zone plate parameters.

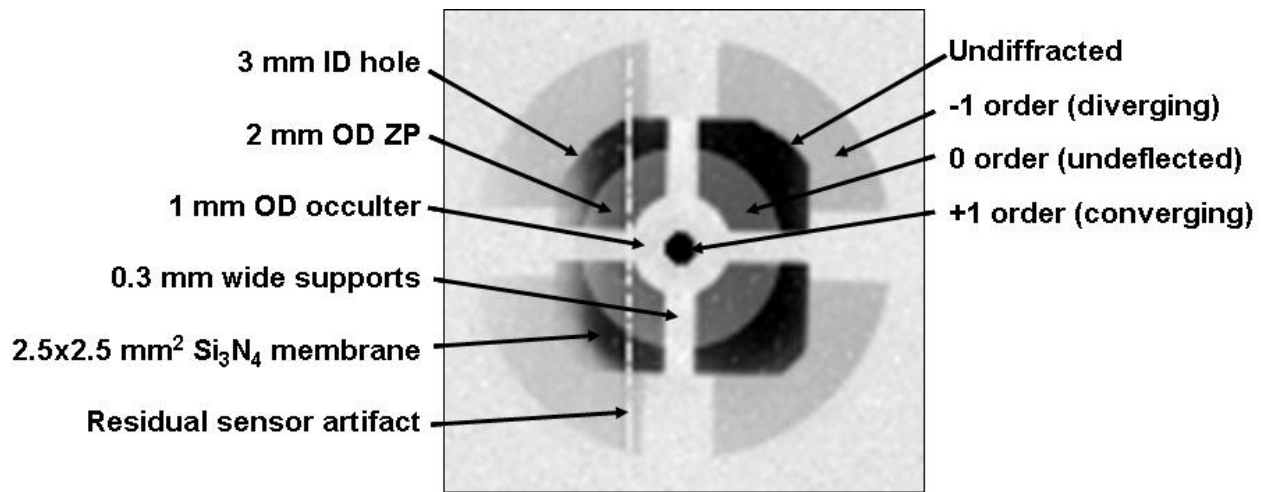


Fig. 4. Diffraction pattern when illuminating the ZP with 13.5 nm radiation.

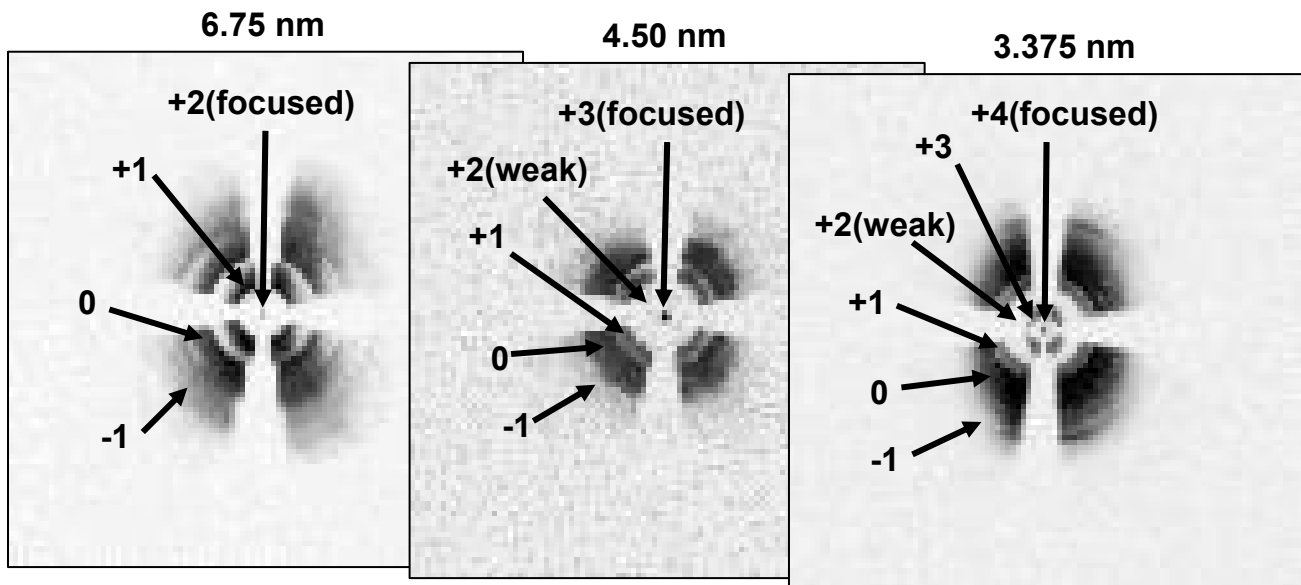


Fig. 5. Diffraction pattern recorded at the 13.5 nm detector distance and for 6.75 nm, 4.50 nm, and 3.375 nm illumination.

Shown in Fig. 5 are images of the complicated higher-order diffraction patterns produced when the ZP was at the 13.5 nm focal distance and was illuminated by second, third, and fourth order wavelengths (6.75 nm, 4.50 nm, and 3.375 nm, respectively). These images were essential for understanding the diffraction patterns and for moving the apertured diode into the desired region of the pattern for efficiency measurements. Figure 5 also illustrates the low efficiency in the even orders, which have zero efficiency for an ideal ZP.

In order to measure the efficiency of the gold zones, it was necessary for the incident radiation beam to underfill the zones and to account for the fractions of the beam intensity passing through the zones outside the occulter. In addition, it

was necessary to account for the transmittance of the  $\text{Si}_3\text{N}_4$  membrane supporting the zones. The fractional beam intensity passing through the zones was determined from images as shown in Fig. 6. A software template was derived from the shadow of the occulter and support spokes, and the template was applied to the direct beam image recorded when the ZP assembly was moved aside. It was determined that 45% of the beam intensity passed through the zones outside the occulter.

The transmittance of the  $\text{Si}_3\text{N}_4$  membrane was measured by passing the beam through the membrane outside the zones and within the 3 mm diameter flexure hole (see Fig. 4). The measured transmittance is shown by the solid curves in Fig. 7. The membrane had a 20 nm thick Ti coating, and the  $\text{Si}_3\text{N}_4$  thickness inferred from the comparison of the measured transmittance and the calculated transmittance (dashed curve in Fig. 7) is 150 nm. This is thicker than the expected 100 nm thickness listed in Fig. 3.

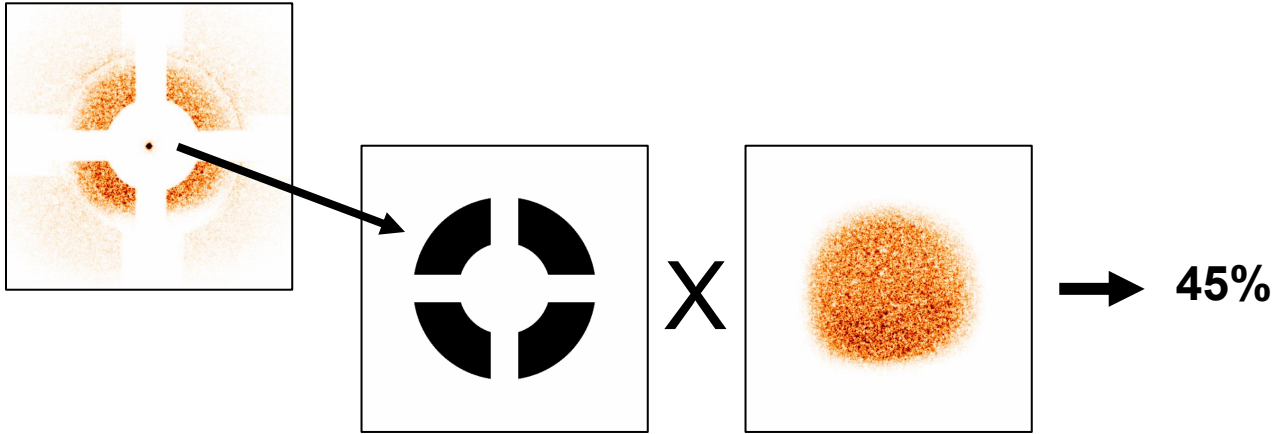
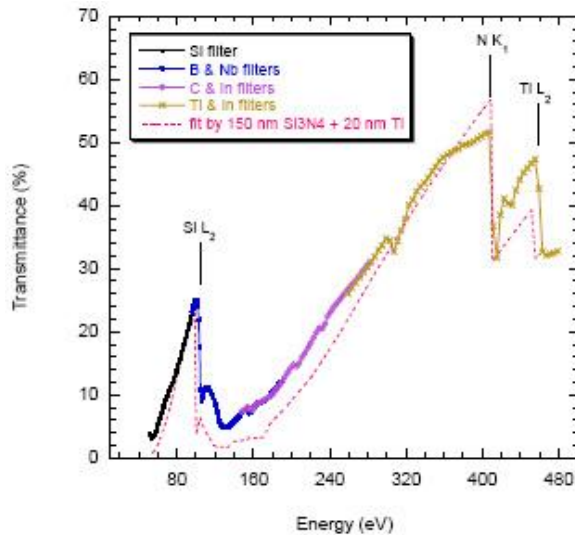


Fig. 6. The software template derived from the shadow of the occulter and supports indicates 45% transmittance of the incident beam.

Fig. 7. Transmittance of the support membrane.



### 3. EFFICIENCY MEASUREMENTS

Wavelength scans were performed using the 0.15 mm apertured diode at a fixed distance from the ZP equal to the focal length of the central wavelength of the scan. As shown in Fig. 8 for the case of 20.0 nm central wavelength, the efficiency curve is approximately trapezoidal in shape. Geometrical ray analysis indicates the widths of the trapezoid top and bottom, divided by the central wavelength, are equal to  $d/R_Z$  and  $d/R_O$  where  $d$  is the detector aperture diameter,  $R_Z$  is the ZP radius, and  $R_O$  is the occulter radius. Thus it is possible to design the wavelength bandpass of a solar monitor using the geometrical parameters of the ZP, detector, and radiation beam.

Using fixed incident wavelength, scans of the detector distance about the wavelength's focal length were performed as shown in Fig. 8, and the geometrical ray considerations are the same. In all cases, it was found that the ZP focal length,  $f=2R_Z\rho/n\lambda$  where  $\rho$  is the width of the outermost zone, was consistent with  $2R_Z\rho=322$  mm-nm rather than the value 300 mm-nm expected from the ZP parameters listed in Fig. 3. Thus detailed measurements of the ZP performance using monochromatic synchrotron radiation are necessary for accurately determining the ZP parameters, and this process is essential for optimizing the solar monitor instrument design and performance.

When a TG is rotated off axis from the incident radiation beam, it is well known that the inside and outside orders, with respect to the rotation, become stronger and weaker, respectively.<sup>5</sup> For example in Fig. 1, when the TG is rotated in the counter-clockwise direction, the indicated order is an outside order and becomes weaker. The same is true of a ZP as illustrated in Fig. 9. In the case of a TG, the signal from a detector placed in an (unfocused) order position varies when the TG is rotated off axis. In contrast, the signal from a detector placed at the ZP focal position and collecting all rays from the ZP (including the purely inside and outside orders indicated in Fig. 8) is constant with off axis angle. This was confirmed by measuring the ZP efficiency in the focused +1 order for off-axis angles up to  $\pm 1^\circ$  and for a number of wavelengths, and example data up to  $\pm 0.5^\circ$  are shown in Fig. 9. In all cases, the focused +1 order efficiency was constant with off-axis angle within the accuracy of the measurements. This is consistent with the ZP circular symmetry and also with efficiency calculations performed using the PCGRATE code.<sup>6</sup>

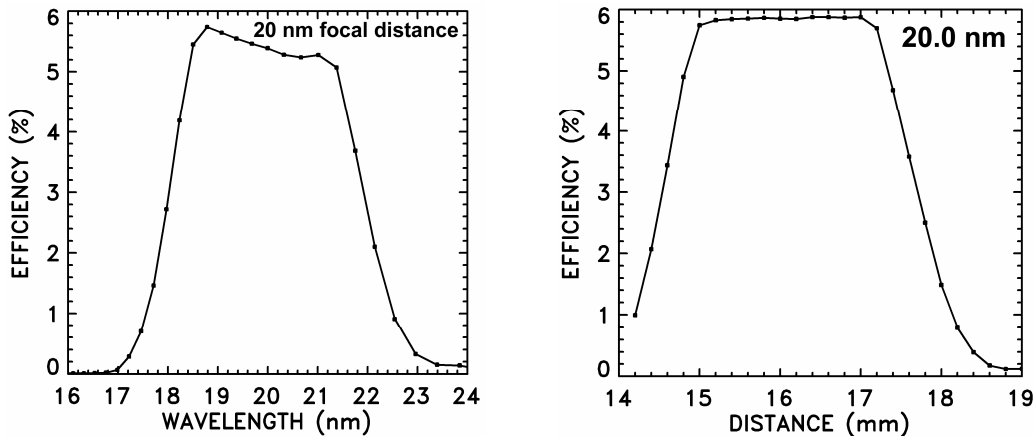


Fig. 8. Left: Wavelength scan at a fixed detector-to-ZP distance equal to the focal length of 20 nm radiation. Right: Detector scan along the ZP axis for 20 nm incident radiation.

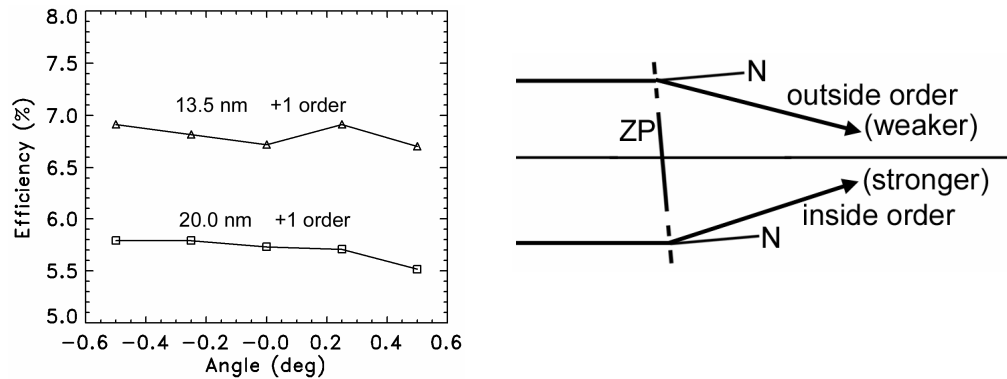


Fig. 9. Left: The measured +1 order efficiency at incident wavelengths of 13.5 nm and 20 nm and for off-axis yaw angles from  $-0.5^\circ$  to  $+0.5^\circ$ . Right: Schematic of the ZP rotated to an off-axis angle.

The GOES-N solar monitors as originally designed and built had one detector per TG channel, and the instrument sensitivity varied with off-axis angle. Since constant sensitivity across the  $0.5^\circ$  solar disk is necessary for the accurate measurement of the total solar emission, and since the longer EUV wavelength C and D channels had inadequate visible light blocking, the C and D channels were subsequently modified to record the A and B wavebands on the opposite sides of the TG axis. Thus when the signals from the detectors on the two sides of the TG axis were summed, for each of the A and B wavebands, the summed signal was independent of off-axis angle. However, the result is that the present modified GOES-N solar monitors do not cover the C and D wavebands with wavelengths 40-65 nm and 65-100 nm, respectively.

In the case of a solar monitor using a ZP, the instrument has no change in sensitivity with off-axis angle, and a single detector can accurately record the emission across the solar disk. Moreover, as discussed in Section 1, the ZP instrument can be designed to cover the 40-100 nm wavelengths as well as other EUV wavebands because of the beneficial ZP focusing properties.

Figure 10 shows the on-axis +1 order efficiency measured over a broad EUV wavelength range from 3.4 nm to 22 nm. PCGRATE modeling indicates the high efficiency peaking at 8.3 nm is a phase-shift enhancement resulting from the partial transmittance of the gold zones as shown in Fig. 11. The calculated wavelength of the peak efficiency varies with gold zone thickness, and the 8.3 nm peak wavelength is consistent with 140 nm zone thickness, less than the expected 180 nm thickness (Fig. 3). However, the absolute values of the calculated peak efficiencies do not exceed 22%, even when varying the zone structure and the gold optical constants over reasonable values, significantly lower than the measured 30% value. Further calculations and measurements, and perhaps a more complete understanding of the ZP structure, are required to understand the cause of this discrepancy.

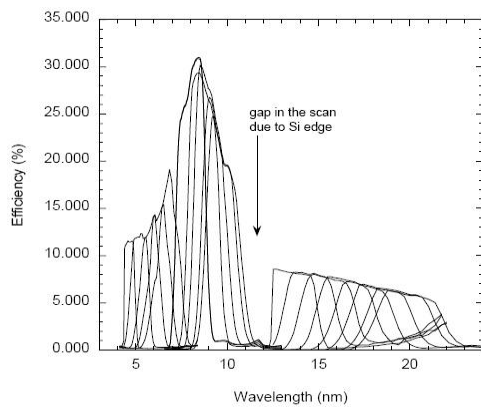


Fig. 10. Measured +1 order on-axis efficiencies.

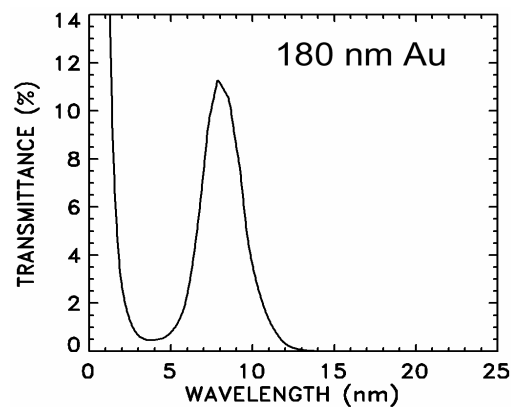


Fig. 11 Transmittance of 180 nm Au.

#### 4. SUMMARY

This work experimentally demonstrates that zone plates can replace the transmission gratings in a GOES-N type solar monitor and can provide superior performance. While the GOES-N solar monitors are already substantially built, the design of solar monitors for the next series of GOES-R solar monitors is under consideration. In order to further demonstrate the flight qualification of zone plates capable of operating at wavelengths as long as 100 nm, it is necessary to replace the Si<sub>3</sub>N<sub>4</sub> support membrane of the presently tested zone plate, which is absorptive at wavelengths longer than approximately 22 nm, with an open mesh support structure similar to the GOES-N flight transmission gratings. A preliminary design of such a support mesh has been carried out, and computer simulations indicate the mesh and the attached ZP can survive launch vibrations. Confirmation that a mesh-supported zone plate can actually survive launch and function in an orbital solar monitor will require ground-based vibration testing and further measurements of the EUV efficiency using monochromatic synchrotron radiation.

**Acknowledgement:** The NRL work was supported by the Office of Naval Research. Swales Aerospace was supported by NASA contract NAS501090. NSLS is operated by the U. S. Department of Energy.

#### REFERENCES

1. J. E. Wise, G. Gaines, A. Gaudet, M. A. Gummin, F. A. Hanser, A. Harris, S. Hersey, and B. Kjornrattanawanich, "GOES Solar EUV Detector Calibration at the NSLS," *SPIE vol. 5549*, 123-133 (2004).
2. J. C. Bremer and W. Yun, "Concept for an extreme ultraviolet sensor with a Fresnel zone plate for the GOES-R Solar Imaging Suite," *SPIE vol. 5901*, 59010P1-12 (2005).
3. J. F. Seely, B. Kjornrattanawanich, G. E. Holland, and R. Korde, "Response of a SiC photodiode to extreme ultraviolet through visible radiation," *Opt. Lett.* *30*, 3120-3122 (2005).
4. J. Hu, X. Xin, J. H. Zhao, F. Yan, B. Guan, J. Seely, and B. Kjornrattanawanich, "Highly sensitive visible-blind extreme ultraviolet Ni/4H-SiC Schottky photodiodes with large detection area," *Opt. Lett.* *31*, 1591-1593 (2006).
5. N. M. Ceglio, A. M. Hawryluk, D. G. Stearns, M. Kuhne, and P. Muller, "Demonstration of guided-wave phenomena at extreme-ultraviolet and soft-x-ray wavelengths," *Opt. Lett.* *13*, 267-269 (1988).
6. Leonid Goray, [www.pcgrate.com](http://www.pcgrate.com)